Revisit to Low Mass Scalar Mesons via Unitarized Chiral Perturbation Theory

M. Uehara*
Takagise-Nishi 2-10-17, Saga 840-0921, Japan

April 3, 2002

Abstract

We study how the scalar mesons below 1 GeV are generated through the Oller- Oset-Peláez version of the multichannel inverse amplitude method applied to the chiral perturbation theory. We find out that the $f_0(980)$ state is generated as a bound state resonance below the $K\bar{K}$ threshold, while the $a_0(980)$ state, generated via the channel coupling between the $\pi\eta$ and $K\bar{K}$ channels, appears as a cusp at the $K\bar{K}$ threshold. The so-called $\sigma(500)$ and $\kappa(900)$ need not be interpreted as the conventional resonances.

@ @ @ @ @ @@ @ @

1 Introduction

Recently, many papers have been appeared on the studies of the scalar mesons below 1 GeV, but it seems that we have still not reached any certain conclusion on their existence and nature as a whole.

The experimental feature of the $(I, J) = (0, 0)$ channel is qualitatively stated as follows: The phase shift makes a plateau near $60^\circ \sim 80^\circ$, and reaches 90° at $800 \sim 900$ MeV and then rapidly increases to exceed 200° near the $K\bar{K}$ threshold, and $\pi\pi$ scattering is almost pure elastic below the $K\bar{K}$ threshold[1, 2]. It is not clear, however, where are the resonant states involving the so-called σ meson in the broad mass distribution from 400 to 1200 MeV denoted as $f_0(400 \sim 1200)$ in the Particle Data Group Lists 2000[3]. The complex pole searches in the $\pi\pi$ scattering amplitude, the attempts to fit the data by the Breit-Wigner formulae or the analyses by using the K-matrix are cited there, but the obtained values are widely spread and seem to depend strongly on the models adopted. On the contrary the $f_0(980)$ state hidden in the structure near the $K\bar{K}$ threshold has the mass converging to a common value near 980 MeV, while its width is spread a little[3].

In the $(I, J) = (1, 0)$ channel a sharp peak is observed near the $K\bar{K}$ threshold[4], which is denoted as $a_0(980)$. But it is still not clear whether $a_0(980)$ is certainly a resonance or a cusp, since the $\pi\eta$ scattering data are scarce. About the $(I, J) = (1/2, 0)$ channel, it is controversial whether the so-called $\kappa(900)$ really exists or not. The phase shift does not exceed 90° below 1GeV at all[5]. This state is not yet cited in the PDG List[3].

The central issue in the $(I, J) = (0, 0)$ channel below 1 GeV is to understand the mechanism to generate the mass distribution such as the broad peak and the dip or steep cliff near the $K\bar{K}$ threshold: Is the σ state really hidden in the broad peak and how the $f_0(980)$ state is generated ? We are also interested in the following issues whether the $a_0(980)$ state is also a bound state resonance like a twin of $f_0(980)$, and whether the πK broad mass peak should be interpreted as the the resonance called by $\kappa(900)$.

In this note we try to analyze the above issues by use of the multichannel Inverse Amplitude Method(IAM) of the Chiral Perturbation Theory[6, 7, 8, 9, 10]. In the IAM of the ChPT a meson-meson scattering amplitude is given as the Padé [1,1] approximant applied to the perturbative amplitudes up to $O(p^4)$ in order to satisfy the $s-$channel unitarity and be applied to the resonance region. The Lagrangian of the ChPT does not incorporate the σ field nor other resonance fields as the independent degrees of freedom

*e-mail: ueharam@cc.saga-u.ac.jp

in advance, and then it offers a good theoretical framework to study the issues. Of course, this does not imply that the existence or nonexistence of a resonance can be completely predicted by the IAM, since the theory contains a set of the phenomenological parameters determined by the experimental data.

Despite the fact that the overall fits have already been given using the full T_4 amplitudes by Goméz Nicola and Pelàez[10], we revisit the issues around the scalar mesons with use of the IAM in order to understand the contents of the fits, that is, how the resonances are generated or not generated. For this purpose we adopt the Oller-Oset-Pelàez (OOP) version of the IAM[9], since the OOP version is much simple and describes rather well the qualitative behavior of the data. The OOP version picks up only the polynomial terms, T_4^P's with the coefficients L_n's and the s-channel loop terms out of the full $O(p^4)$ amplitudes, neglecting the left hand singularities. It may be said that the OOP version is like the K-matrix approximation to the full amplitude.

The conclusion on the scalar mesons viewed from the OOP version of the 2×2 channel IAM is summarized as follows:

1. The nonet structure of the scalar mesons below 1 GeV does not hold.
2. The $f_0(980)$ state is a typical example of the bound state resonance[11, 12]: The $K\bar{K}$ scattering amplitude has a bound state pole on the real axis, if the channel coupling is switched off, and the channel coupling moves the pole into the second sheet and generates the resonant behavior near the $K\bar{K}$ threshold. But its explicit resonant form is hidden in the large $\pi\pi$ background.
3. If we take the parameter set adopted in this note, the $a_0(980)$ state appears as the strong cusp, not as the resonance. The origin of $a_0(980)$ is not the $K\bar{K}$ bound state pole but the channel coupling between the $\pi\eta$ and $K\bar{K}$ channels. This gives a sharp peak at the $K\bar{K}$ threshold, but the elastic $\eta\pi$ phase shift cannot exceed 90° below the $K\bar{K}$ threshold.
4. The broad peak of the isoscalar-scalar $\pi\pi$ mass distribution centered at 500 MeV need not be interpreted as the conventional resonance. It represents the attractive interaction between two pions with the vacuum quantum number corresponding to the vacuum fluctuation coming from the spontaneous symmetry breaking. The $\kappa(900)$ state is also not the conventional resonance similar to σ.

The mechanism to generate $f_0(980)$ and $a_0(980)$ is similar to the $K\bar{K}$ molecule model discussed by Weinstein and Isgur using the nonrelativistic quark model[13] and Jülich group using the meson exchange models[14, 15], though our theoretical framework is much different from theirs.

This paper is organized as follows: We briefly explain the Oller-Oset-Pelàez version in the next section. The scalar mesons are discussed in Sec.3 and the vector resonances in Sec. 4. Concluding remarks and discussion are given in the last section.

2 The amplitudes in the IAM

Since the derivation of the IAM applied to the ChPT has been given in Refs.[6, 7, 8, 10], here we summarize the amplitudes in the OOP version[9]. In this note we take the two-channel model. The partial wave amplitudes in the two-channel IAM to $O(p^4)$ are written as

$$\boldsymbol{T}(w) = \boldsymbol{t}_2(w)[\boldsymbol{t}_2(w) - \boldsymbol{t}_4(w)]^{-1}\boldsymbol{t}_2(w), \tag{2.1}$$

where $\boldsymbol{t}_2(\boldsymbol{t}_4)$ is the partial wave amplitude with chiral order $O(p^2)$ ($O(p^4)$) amplitude given by the symmetric 2×2 matrix and w is the total CM energy. Our T-matrix is related to S-matrix as

$$S_{ij}(w) = \delta_{ij} - 2i\rho_i^{1/2}(w)T_{ij}(w)\rho_j^{1/2}(w), \tag{2.2}$$

$$\rho_i(w) = \frac{1}{16\pi}\frac{2k_i}{w} \tag{2.3}$$

where ρ_i is the phase space factor with k_i being the CM momentum in the i-th channel.

Instead of taking the full $T_4(s,t,u)$, which involves the left-hand cut coming from the $t-$ and $u-$channel loop diagrams, the OOP version picks up only the s-channel loop diagrams and the polynomial terms written as $T_4^P(s,t,u)$ with the phenomenological coefficients L_n's left after the renormalization of the one-loop diagrams[16, 17]. All of our $T_4^P(s,t,u)$ are taken from the Ref. [10]. Thus, the partial wave $\boldsymbol{t}_4(w)$ is given as

$$\boldsymbol{t}_4(w) = \boldsymbol{t}_4^P(w) + \boldsymbol{t}_2(w)\cdot\boldsymbol{G}(w)\cdot\boldsymbol{t}_2(w), \tag{2.4}$$

where $\boldsymbol{t}_4^P(w)$ is the partial waves coming from $T_4^P(s,t,u)$, and $\boldsymbol{G}(w)$ is the diagonal 2×2 loop integral under the $\overline{MS}-1$ regularization [16]. $G_i(w)$ in the $i-$th channel is written as

$$G_i(w) = \frac{1}{(4\pi)^2}\left\{-1+\log\left(\frac{m^2}{\mu^2}\right)+\sigma_i(w)\log\left(\frac{\sigma_i(w)+1}{\sigma_i(w)-1}\right)\right\}, \tag{2.5}$$

$$\sigma_i(w) = \sqrt{1-4m^2/w^2} = \frac{2k_i}{w} \tag{2.6}$$

for the channel with the equal mass m in the $i-$th channel, and k_i is the CM momentum, and

$$\begin{aligned} G_i(w) &= \frac{1}{(4\pi)^2}\left\{-1+\log\left(\frac{m_1m_2}{\mu^2}\right)+\frac{\Delta_{21}}{w^2}\log\left(\frac{m_2}{m_1}\right)\right. \\ &+ \left.\lambda_i(w)\log\left(\frac{\sigma_{i+}(w)+\sigma_{i-}(w)}{\sigma_{i+}(w)-\sigma_{i-}(w)}\right)\right\}, \end{aligned} \tag{2.7}$$

$$\sigma_{i\pm} = \sqrt{1-(m_1\pm m_2)^2/w^2}, \tag{2.8}$$

$$\lambda_i(w) = \sigma_{i+}(w)\sigma_{i-}(w) \tag{2.9}$$

for the channel with unequal masses m_1 and m_2 in the $i-$th channel, and $\Delta_{21}=m_2^2-m_1^2$. The imaginary part of $G_ii(w)$ is given as

$$\mathrm{Im}G_i(w) = -\frac{1}{16\pi}\frac{2k_ii}{w}\theta(w-w_i) \equiv -\rho_i(w) \tag{2.10}$$

with w_i is the threshold energy of the $i-$th channel.

Although the full amplitudes T_2 and T_4 satisfy the crossing symmetry, it is known that the unitarized amplitudes projected on the definite (I,J) channel of the $s-$channel break the crossing symmetry. The amplitudes of the OOP version could break it more largely, since the version discards the $t-$ and $u-$channel loop diagrams.

The OOP version of the multichannel IAM is just like the K-matrix formalism, which ignores the lefthand cut of the scattering amplitudes. Defining the K-matrix as

$$\boldsymbol{K} = \boldsymbol{t}_2[\boldsymbol{t}_2 - \mathrm{Re}(\boldsymbol{t}_4(w))]^{-1}\boldsymbol{t}_2, \tag{2.11}$$

where $\boldsymbol{t}_4$ is the OOP version given by Eq.(2.4), we rewrite the OOP version of the IAM amplitude as

$$\boldsymbol{T} = \boldsymbol{K}[1+i\boldsymbol{\rho}\cdot\boldsymbol{K}]^{-1}. \tag{2.12}$$

$\boldsymbol{K}$ in Eq.(2.11) is real analytic as the usual K-matrix.

Since the OOP $\boldsymbol{t}_4$ discards the contributions from the left hand cut, the results would be different from those obtained by using the full T_4 amplitudes under the same set of the coefficients L_n's[19]. Thus, we relax the values of L_n's obtained in ref.[10] in order to reproduce the characteristic features of the scattering amplitudes. We adopt the parameter set of $\hat{L}_n\times 10^3$ shown in Table 2, which is compared with the set of ref.[10] cited as GNP and the one-loop ChPT set obtained in 1995[18]. Note that while the GNP and the ChPT sets are determined at $\mu=M_\rho$, we take $\mu=1$ GeV. This is because a little larger μ is easy to reproduce the qualitative behavior of the $(I,J)=(0,0)$ channel. The original OOP version took the momentum cutoff corresponding to $\mu=1.2$ GeV[9]. For the vector meson channel much larger μ can give better results.

It should be stressed that our present set is not the best choice to fit the experimental data: Indeed, we fail to reproduce the isospinor πK scattering amplitude below 770 MeV. It is interesting, however, that our set is not far from the GNP and ChPT sets.[1]

[1]Other sets of $\hat{L}_n$'s in refs.[9, 8] are not quoted, because their amplitudes are different from those of ref.[10].

	$\hat{L}_1$	$\hat{L}_2$	$\hat{L}_3$	$\hat{L}_4$	$\hat{L}_5$	$\hat{L}_6$	$\hat{L}_7$	$\hat{L}_8$
GNP	0.56	1.21	-2.79	-0.36	1.4	0.07	-0.44	0.78
Ours	0.51	1.11	-2.95	-0.35	1.5	-0.2	-0.4	0.89
ChPT	0.4 ± 0.3	1.35 ± 0.3	-3.5 ± 1.1	-0.3 ± 0.5	1.4 ± 0.5	-0.2 ± 0.3	-0.4 ± 0.2	0.9 ± 0.3

Table 1: $\hat{L}_n \times 10^3$

Now, we summarize the notations used in the following sections. We divide $D_{ij} = [\boldsymbol{t}_2 - \boldsymbol{t}_4]_{ij}$ into the real and imaginary part as

$$D_{ij}(w) = a_{ij} + i(\rho_1 b^1_{ij} + \rho_2 b^2_{ij}), \tag{2.13}$$

where

$$\begin{aligned} a_{ij} &= (\boldsymbol{t}_2)_{ij} - (\boldsymbol{t}_4^P)_{ij} - (\boldsymbol{t}_2 \boldsymbol{g}(w) \boldsymbol{t}_2)_{ij}, & (2.14)\\ b^k_{ij} &= (\boldsymbol{t}_2)_{ik}(\boldsymbol{t}_2)_{kj} & (2.15) \end{aligned}$$

with $\boldsymbol{g}(w) = \mathrm{Re}\boldsymbol{G}(w)$. Thus, $T_{ii}(w)$, the elastic scattering amplitude of the i-th channel, is written as

$$\rho_i T_{ii}(w) = \frac{B_i(w) + iC(w)}{A(w) + i[B_1(w) + B_2(w)]}, \tag{2.16}$$

where

$$\begin{aligned} A(w) &= a_{11}a_{22} - a_{12}^2 - C(w), & (2.17)\\ B_1(w) &= \rho_1[a_{11}b^1_{22} + a_{22}b^1_{11} - 2a_{12}b^1_{12}], & (2.18)\\ B_2(w) &= \rho_2[a_{11}b^2_{22} + a_{22}b^2_{11} - 2a_{12}b^2_{12}], & (2.19)\\ C(w) &= \rho_1\rho_2[b^1_{11}b^2_{22} + b^1_{22}b^2_{11} - b^1_{12}b^2_{12}]. & (2.20) \end{aligned}$$

The $i-$th channel amplitude $\hat{T}_{ii}$ in the single channel problem is given as

$$\rho_i \hat{T}_{ii}(w) = \frac{\rho_i b^i_{ii}}{a_{ii} + i\rho_i b^i_{ii} + i\rho_j b^j_{ii}}, \tag{2.21}$$

where we note that a_{ii} contains the meson loops not only of the $i-$th channel but also of the other $j-$th channel.

The S-matrix for the first channel with the lower threshold energy is written as

$$S_{11} = \frac{A + 2C - i(B_1 - B_2)}{A + i(B_1 + B_2)} = \eta(w)\exp[2i\delta_1(w)], \tag{2.22}$$

where the phase shift $\delta_1(w)$ and the inelasticity $\eta(w)$ are calculated through this definition.

3 Scalar mesons

We study how the scalar mesons are generated through the IAM applied to ChPT. Since we need qualitative behavior of the amplitudes, we do not cite any experimental data to compare the calculated results. The definitions of the amplitudes have been given in Eqs.(2.14), (2.15), (2.17), (2.20), (2.18),(2.19). We calculate up to 1.2 GeV within the OOP version of the two-channel IAM, but we should note that the $\eta\eta$ channel and higher resonances may affect the results even below 1.2 GeV.

3.1 The (I,J)=(0,0) channel: $\pi\pi \times K\bar{K}$

The characteristic behavior of this channel is that the phase shift $\delta_{00}(w)$ rises from the $\pi\pi$ threshold, forms a plateau of $60^\circ \sim 80^\circ$ from 500 to 800 MeV, crosses 90° in the region 800 $\sim$ 900 MeV, and suddenly increases to exceed 200°just below the $K\bar{K}$ threshold. The behavior implies that $A(w)$ defined

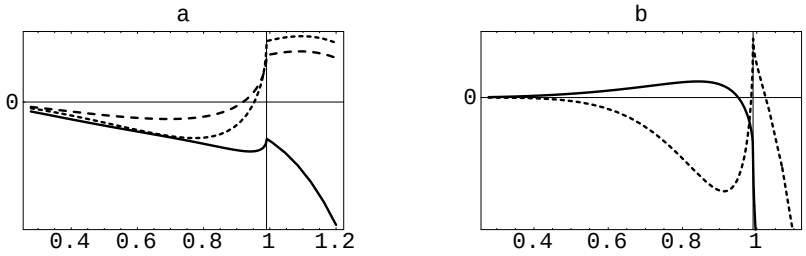

Figure 1: Energy dependence of $a_{ij}(w)$. (a) a_{11} is given by the solid line, a_{22} by the dotted line and a_{12} by the dashed line. (b) Energy dependence of the resultant amplitude. The real part, A, is given by the solid line and the imaginary part,$B_1 + B_2$, by the dotted line.

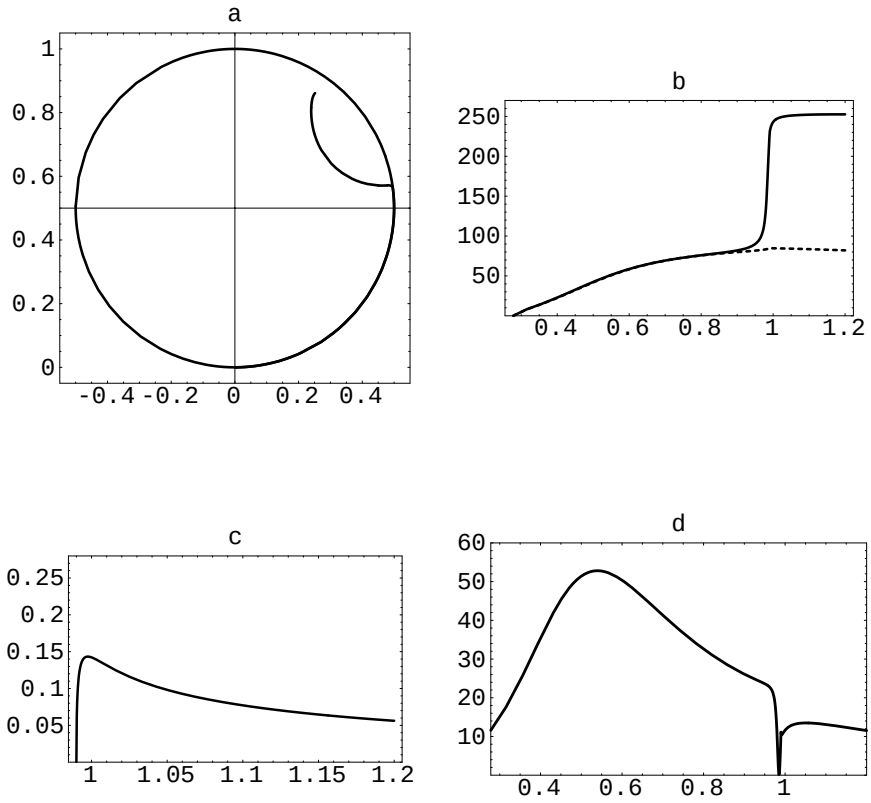

Figure 2: (a) Argand diagram starting at the $\pi\pi$ threshold, drawing the circle and bending at $K\bar{K}$ threshold.. (b) Phase shift δ_{00} given by solid line, and the single channel phase shift by dotted line. (c) Absorption rate, $(1-\eta_{00}^2)/4$. (d) The $\pi\pi$ cross section in mb.

by Eq.(2.17), the real part of denominator of $T_{11}(w)$, should develop a zero at the point where δ_{00} goes across 90° and $B_1(w)$ of Eq.(2.18), the imaginary part, does so at very close to the $K\bar{K}$ threshold.

At first we observe from Fig.1(a) that $a_{22}(w)$ develops a zero. This zero stays below the $K\bar{K}$ threshold, if we eliminate the pion-loop contribution in $a_{22}(w)$. This means that there is the bound state pole in the isolated $K\bar{K}$ channel, which generates the bound state resonance in the $\pi\pi$ scattering amplitude with

$(I, J) = (0, 0)$ state. The bound state pole moves into the second complex sheet near the real axis as the channel coupling is switched on. The nearby pole appears as the zero of $A(w)$. The zero of $B_1(w)$ is also due to the zero of $a_{22} \cdot b_{11}^1$ primarily, but the remaining negative terms push the zero closer to the $K\bar{K}$ threshold. It is noted, however, that the negative terms are required to be not so large in order to maintain the zero in B_1. If B_1 does not develop the zero, the resultant phase shift cannot exceed 180°. Thus, the sudden rise of the phase shift is not the simple result of the bound state pole in the $K\bar{K}$ channel. This mechanism to generate the bound state resonance below $K\bar{K}$ threshold is similar to the one discussed by Weinstein and Isgur[13] and Jülich group[14, 15], though the theoretical framework of the IAM is quite different from theirs.

We show the results on the Argand diagram, the phase shift δ_{00}, the absorption rate $[1 - \eta_{00}^2]/4$ and the $\pi\pi$ cross section in Fig.2 (a), (b) and (c), respectively. Our calculation reproduces the characteristic features qualitatively, and gives the results very similar to those by the full amplitude calculation[10].

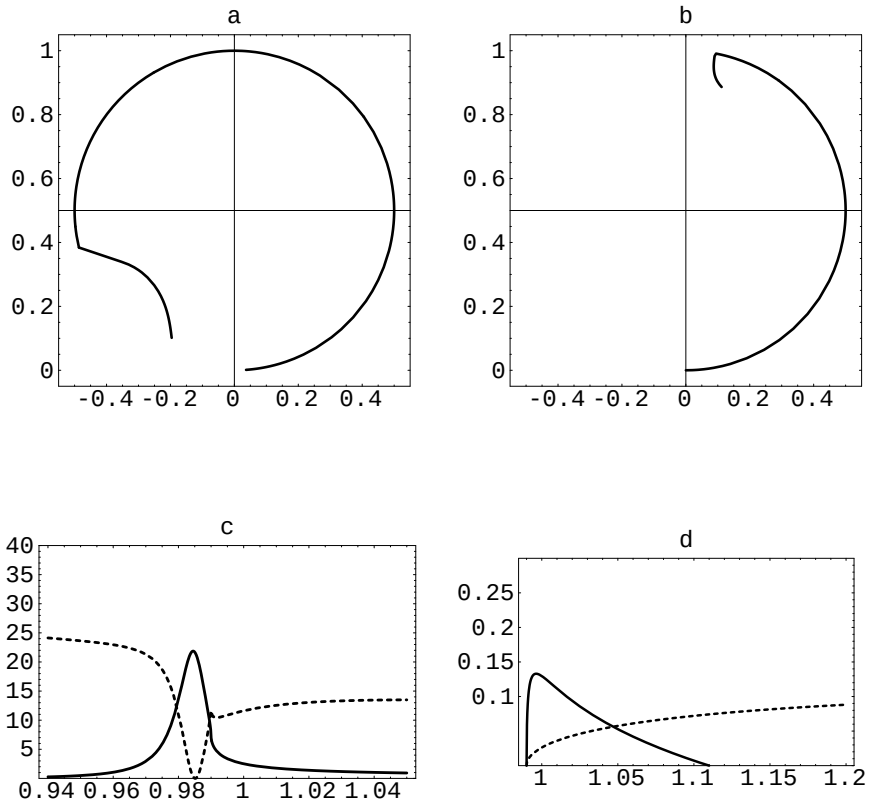

Figure 3: (a) The Argand diagram of f_0 amplitude from 900 to 1050 MeV. (b) The Argand diagrams of $\hat{T}_{11}$ from the $\pi\pi$ threshold to 1.2 GeV. (c) The solid line shows the sharp Breit-Wigner peak of the the f_0 state extracted by Eq.(3.1), dotted line does the full cross section, and (d) The absorption rate $(1 - \eta_{00})^2)/4$ of $f_0(w)$ is given by the solid line and the one of the "background" by the dotted line.

Now, in order to extract the $f_0(980)$ behavior explicitly we define the f_0 amplitude through the following formula;

$$T_{11}(w) = \hat{T}_{11}(w) + f_0(w) \exp[2i\hat{\delta}_{11}(w)], \tag{3.1}$$

which is the Dalitz-Tuan prescription widely used to unitarize the sum of the two scattering amplitude[11]. Here $\hat{T}_{11}$ is the single channel $\pi\pi$ amplitude with $\hat{S}_{11} = 1 - 2i\hat{T}_{11}$ defined in Eq.(2.21). $\hat{T}_{11}$ cannot draw a full circle in the energy range to 1.2 GeV and plays a role of the background to $f_0(w)$. We observe

that a sharp peak of the f_0 state hidden in the $\pi\pi$ cross section appears like the typical Breit-Wigner resonance as shown in Fig.3 (a) and (c), and that the strong rise of the absorption rate $(1-\eta_{00}^2)/4$ just above the $K\bar{K}$ threshold should be attributed to the resonant behavior of the f_0 amplitude as shown in Fig.3 (d). The f_0 amplitude could be approximated by the Breit-Wigner form,

$$f_0(w) = \frac{m_0\Gamma_1}{m_0^2 - s + im_0(\Gamma_1+\Gamma_2)} \quad \text{with } \Gamma_i = g_i^2 w\rho_i, \tag{3.2}$$

where m_0 is the mass of f_0, $g_1(g_2)$ the scalar coupling constant to $\pi\pi\,(K\bar{K})$. In order to reproduce the sharp rise of the absorption rate just above the $K\bar{K}$ threshold, the ratio g_2^2/g_1^2 is required to be large as the mass m_0 leaves the $K\bar{K}$ threshold. We find that $m_0 \sim 985$ MeV, $g_1^2 \sim 0.5$ and $g_2^2/g_1^2 \sim 10$ in our set of the parameters, but the detailed values of the mass and width are too model-dependent and cannot be trusted. At least it would be certain that f_0 behaves like the Breit-Wigner resonance with the large $K\bar{K}$ coupling constant.

The rising and plateau of the phase shift and the falling behavior of the kinematical limit of the cross section, $4\pi/k^2$, shape the $\pi\pi$ cross section into the broad peak from $400 \sim 800$ MeV, peaked at 500 MeV, as shown in Fig.2 (d). We show also that the phase shift below 800 MeV is almost similar to that of the single channel $\hat{T}_{11}$, and that $\hat{T}_{11}$ cannot draw the full Argand circle up to 1.2 GeV. This behavior is generated essentially by chiral symmetry and unitarity[20], and we do not need any mechanism to hide a conventional resonance in the broad peak. Such a strong two-pion correlation may be called the σ state, but it needs not be expressed by an unstable particle as in the linear σ model, or by a Breit-Wigner formula.

3.2 The (I,J)=(1,0) channel: $\pi\eta \times K\bar{K}$

The a_{22} amplitude has a zero similar to the (0,0) channel, but we note that there are large differences; the amplitude a_{11} is weak repulsive, the $\pi\eta \to (K\bar{K})_{I=1}$ amplitude a_{12} is large, and the zero has disappeared in the resultant amplitude A contrary to the (0,0) channel. Where does the zero disappear ? In order to see the role of the channel coupling including the $\pi\eta$ loop in a_{22} and $K\bar{K}$ loop in a_{11}, we introduce a scale factor α as $\alpha(t_2)_{12}$ and $\alpha(t_4)_{12}$. We observe that the zero of $a_{22}(w)$ does not develop at $\alpha = 0$, that is, there is not a bound state pole. When increasing α gradually, the cusp behavior becomes remarkable and then the cusp changes to the resonance for a sufficiently large α. Such a behavior was studied using a much simpler model in [12], where the complex pole pole starts from the boundary between the third and fourth sheets at $\alpha = 0$, moves to the fourth sheet producing the cusp behavior as α increases, and then appears in the second sheet as the resonance pole. At $\alpha = 1$ in our $(1,0)$ channel, the pole stays in the fourth sheet near the boundary of the second sheet , and then the strong cusp behavior is left. The real part of the complex pole is larger than $2m_K$. The cusp gives a sharp peak of the $\pi\eta$ cross section, the shape of which is not expressed by the Breit-Wigner form as shown in Fig. 5(d).

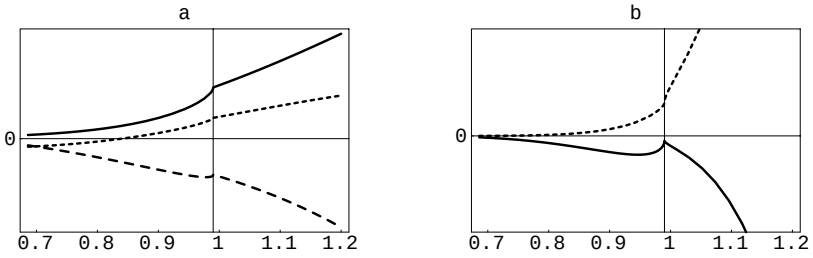

Figure 4: Energy dependence of the amplitudes. (a) a_{11} is given by the solid line, a_{22} by the dotted line and a_{12} by the dashed line. (b) A is given by the solid line and $B_1 + B_2$ by the dotted line.

The large $\pi\eta \to (K\bar{K})_{I=1}$ amplitude drags T_{11} toward the center in the Argand diagram above the $K\bar{K}$ threshold as shown in Fig.5 (a), and the phase shift increases to pass 90° *above* the $K\bar{K}$ threshold.

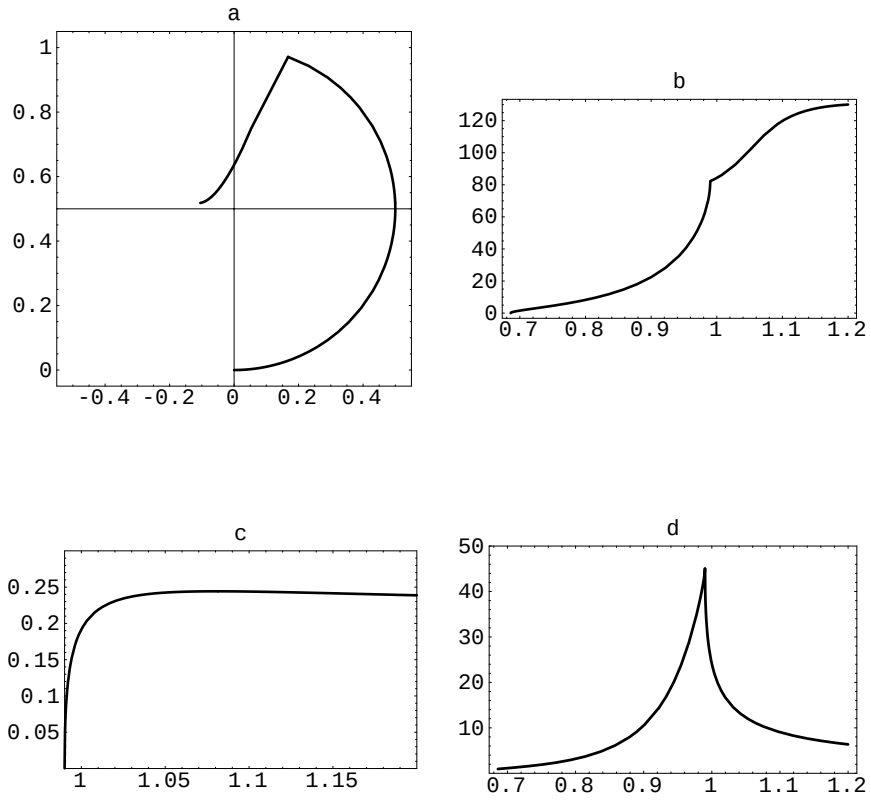

Figure 5: (a) Argand diagram. (b) Phase shift δ_{10}. (c) The production rate. (d) The $\pi\eta$ cross section in units of mb.

The behavior of the phase shift above the $K\bar{K}$ threshold does not imply the existence of a resonance above the $K\bar{K}$ threshold, however. It is also noted that the form of the absorption rate $(1-\eta_{10}^2)/4$ is quite different from the one of the resonant $f_0(980)$ state which shows the sharp rising just above the $K\bar{K}$ threshold. Although it is not clear that the full T_4 calculation reached the same cusp behavior because of the lack of the figure of the phase shift, we point out that the cross section behaves very similarly to our result[10].

It is interesting to note that our result resembles the Jülich model[15], where they state that the a_0 state is essentially generated by the channel coupling without any origin in the diagonal amplitudes, both $\pi\eta$ and $K\bar{K}$ channels. They seem to choose finally the parameters so that the pole is brought to the second sheet off the fourth sheet and then the round shaped $\pi\eta$ cross section is obtained.

3.3 $(I, J,) = (1/2, 0)$ channel: $\pi K \times \eta K$

The experimental πK phase shift increases smoothly up to the ηK threshold without any remarkable structure, but does not exceed 90°[5]. This behavior implies that there is not hidden any conventional resonant structure.

Due to the wrong sign of the ηK elastic amplitude r_{22} at low energies below 760 MeV, both of the A and B_1 have the wrong sign, but we can reproduce the above experimental behavior roughly above 770 MeV. The failure is directly due to the fact that the leading $\eta K \to \eta K$ amplitude $(t_2)_{22}$ behaves as if it has a bound state zero at a low energy and t_4 cannot remove the zero. This would be due to the OOP version with our set of parameters L_n's, since the calculation by the full amplitudes gives the nice result[10]. The Argand diagram shows that the amplitude stops in the second quadrant at ηK threshold, and the phase shift increases up to about 80°, which is a little larger than the data, but does not exceed

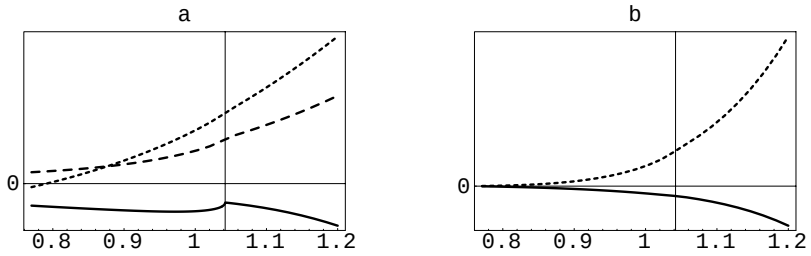

Figure 6: Energy dependence of the amplitudes. Lines are the same as previous Figs.

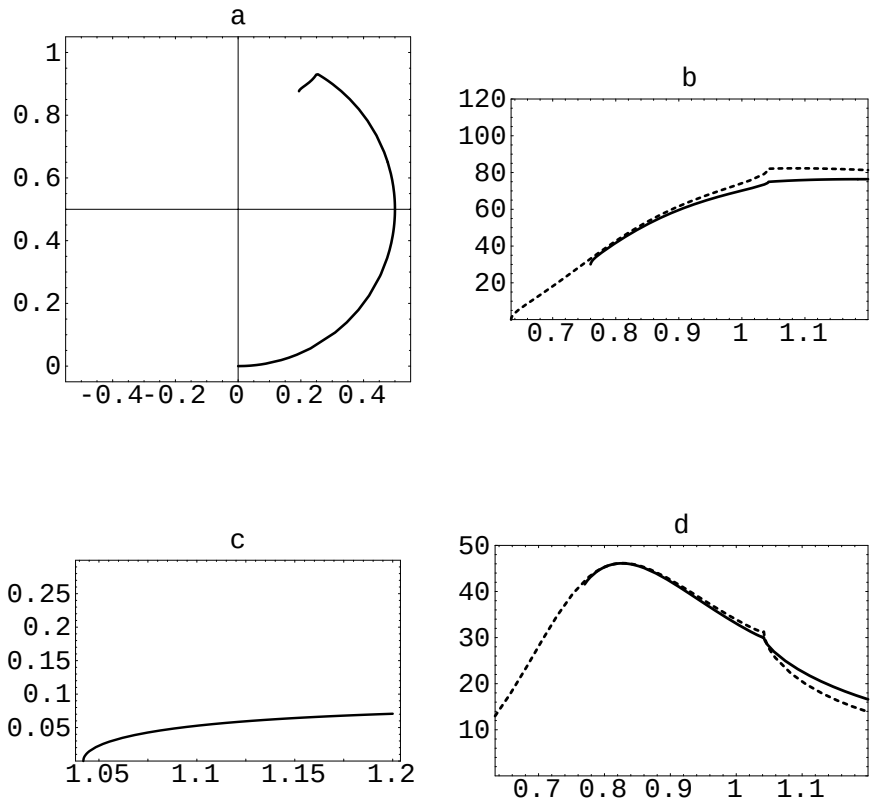

Figure 7: (a) Argand diagram. (b) Phase shift $\delta_{\frac{1}{2}0}$ The solid line is the multichannel calculation, and the dotted one for the single channel calculation. (c) The production rate. (d) The πK cross section.

90° below 1.2 GeV. The Argand diagram up to 1.2 GeV is similar to the result in Ref.[21]. The phase shift by the single πK amplitude is very similar to the multichannel one at higher energies as shown in Fig.7(b). This fact and the rather small absorption by the ηK channel indicate that the effects of the channel coupling seems to be small as contrasted with the $f_0(980)$ and $a_0(980)$ cases. The πK cross section has the large broad peak centered at 850 MeV.

It is certain that both the calculation and experimental data in the (1/2,0) channel lead to the conclusion that that the so-called κ represents the strong πK correlation, but not the conventional resonance. The absence of this state is argued in Refs.[22, 23, 21].

3.4 $(I, J) = (2, 0)$ and $(3/2, 0)$ exotic channels

The $\pi\pi_{(2,0)}$ channel is repulsive, and the phase shift goes down as shown in Fig.3.4(a). Similarly, the πK channel gives the negative $(3/2, 0)$ phase shift, which is shown in Fig.3.4(b). These behaviors are very similar to those of ref.[10], and to the experimental data.

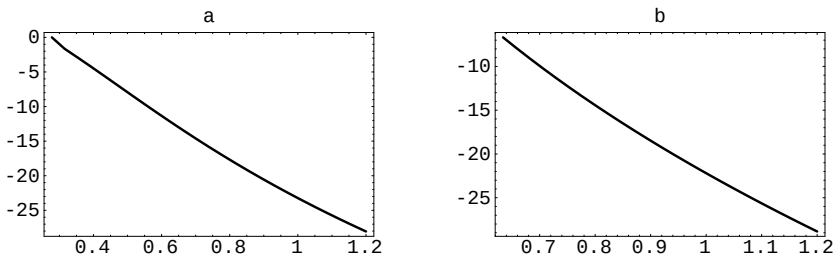

Figure 8: (a) $\delta_{(2,0)}$. (b) $\delta_{(3/2,0)}$.

3.5 Scattering lengths

Here we summarize the scattering lengths of $(I, J) = (0, 0)$, $(2, 0)$, $(1/2, 0)$ and $(3/2, 0)$ channels in unit of $1/m_\pi$:

$$\begin{aligned} a_{(00)} &= 0.214, & a_{(10)} &= 0.029 \qquad a_{(1/2,0)} = /, \\ a_{(2,0)} &= -0.040, & a_{(3/2,0)} &= -0.057. \end{aligned}$$

While the value $a_{(1/2,0)}$ cannot be trusted by the situation stated in the previous subsection, the πK single channel calculation gives a good value, $a_{(1/2,0)} = 0.219$. The channel coupling also changes the scattering length given by the single $\pi\eta$ channel calculation in the $(1, 0)$ channel. The scattering lengths by the one-loop ChPT to $\pi\pi$ scattering[24] and πK scattering under the condition $f_\pi = f_K$[17] are as follows:

$$\begin{aligned} a_{(00)} &= 0.201 & a_{(2,0)} &= -0.041, \\ a_{(1/2,0)} &= 0.19 & a_{(3/2,0)} &= -0.05, \end{aligned}$$

which are close to our calculations, if we take the single channel result for $a_{(1/2,0)}$.

4 Vector mesons

We do not attempt to reproduce the resonance masses exactly, but we think that it is enough for our aim to reproduce them within the error of a few tens MeV .

We define the kinematical singularity free amplitudes $t_{ij}(w)$ as

$$T_{ij}(w) = k_i \cdot t_{ij}(w) \cdot k_j, \tag{4.1}$$

where k_i is the CM momentum in the $i-$th channel. This replacement induces the extra momentum dependence on $\boldsymbol{G}$ as

$$\boldsymbol{G}_i(w) \quad \rightarrow \quad G_i^P(w) = k_i^2 G_i(w). \tag{4.2}$$

Then, the phase space factor ρ becomes

$$\rho_i^P(w) = k_i^2 \rho_i(w). \tag{4.3}$$

		single	multi	Exp. value
ρ	Mass(MeV)	796.9	795.6	769.3 ± 0.8
	Width(MeV)	165.8	165.2	150.2 ± 0.8
K^*	Mass(MeV)	885.2	859.9	891.7 ± 0.3
	Width(MeV)	40.1	36.5	50.8 ± 0.9
"ϕ"	Mass(MeV)	887.9		926.5

Table 2: Masses and widths of the vector resonances both in the single and multichannel formalism.

At first, we observe that the vector meson resonances are realized even in the single channel formalism, and that the channel coupling do not affect the result so much, if the parameter set $\hat{L}_n$'s is selected appropriately. We tabulate the results at $\mu = 1$ GeV in Table 4. As to the $phi(1020)$ meson Ref.[10] gives 935 MeV by use of the full T_4, and they argue that this state is the SU(3) octet part of the ϕ meson, because $P-$wave $K\bar{K}$ state can couple only to the SU(3) octet state, the mass of which is given as 926.5 MeV by using the experimental masses of the vector mesons[25]. If we take this value as the experimental mass of "ϕ", the deviation of our results from the experimental mass values of the vector meson remains within ± 40 MeV. Since the value of the width depends almost linearly to the mass value, the calculated width is large by about 10% for the ρ meson and small by 30% for the K^* meson compared to the experimental one, respectively. If we use the experimental mass values, the calculation gives the ρ width 154.2 MeV and K^* 45.8 MeV, the both of which are reasonable.

In the vector meson channels both for the ρ and K^*, all of the $a_{ij}(w)$ amplitudes cross the zero at almost similar energy. Order of the positions of the zeros in the rho channel is different from those in the K^* channel. This is the reason why the mass in the multichannel is so close to the one in the singlechannel for the ρ channel, but large for the K^* channel. The subtle positions of the zeros depend on the parameter set $\hat{L}_n$'s, but the developing of the zeros in all of a_{ij} would be stable. The developing of the common zeros is the remarkable difference from the scalar channels.

5 Concluding remarks

We have calculated the two-meson scattering amplitudes, mainly in the scalar channel, within the OOP version of the IAM to the ChPT. We used the T_4^P amplitudes calculated by Gomés Nicola and Pelàes[10] with our set of the phenomenological constants $\hat{L}_n$'s given in Table I.

We have arrived at the following conclusion on the low mass scalar meson spectroscopy.

1. The nonet structure of the scalar mesons below 1 GeV does not hold.
2. The $f_0(980)$ state is generated through the bound state appearing in the $K\bar{K}$ channel, and behaves as like as the Breit-Wigner resonance, if we extract the f_0 amplitude from the $\pi\pi$ background.
3. The $a_0(890)$ state is born through the channel coupling between the $\pi\eta$ and $K\bar{K}$ channels, and finally grows up to be the strong cusp.
4. The broad peak centered at 500 MeV, which may be called the σ *state*, is interpreted as the $\pi\pi$ strong correlation coming from chiral symmetry and unitarity, and there is no conventional resonance below 900 MeV.
5. Unfortunately, we failed to reproduce the low energy behavior of the $(I, J) = (1/2, 0)$ channel below 760 MeV, but the calculation with the full amplitudes[10] and the experimental data strongly suggest the conclusion that the $\kappa(900)$ peak need not be the resonance.
6. The $K\bar{K}$ correlation is attractive and so strong as to generate the bound state by $K\bar{K}$ loop alone in the isoscalar channel.

It is impossible, however, to extract any information on the quark contents of the resonances from the analyses by the unitarized ChPT. Even if our conclusion on the mechanism of the generation of $f_0(980)$ and $a_0(980)$ is similar to Refs.[13, 14, 15], we cannot say whether they are the $qq\bar{q}\bar{q}$ or the $K\bar{K}$ molecule. If the $f_0(980)$ appears the resonance but $a_0(980)$ the cusp by the hadronic dynamics, the $q\bar{q}$ scalar nonet should be attributed to the scalar resonances above 1 GeV.

Recently the complex pole search of the amplitudes on the unphysical sheets has been widely attempted in the study of the scalar meson spectroscopy. We have also discussed the movement of the complex poles of the $f_0(980)$ and $a_0(980)$ states . The complex pole is expected to be fundamental, parameterization- and process-independent, but the pole search is performed practically by use of a *model* amplitude, which is parameterized to *fit the data on the real axis approximately*, and then the pole position is the more model-dependent as it is the more distant from the real axis like the σ and κ cases[27].

For example, it is shown that the amplitude coming from the $t-$ and $u-$channel ρ meson exchange in the (0,0) channel develops the complex pole distant from the real axis at (370$-$356i) MeV, for example[29], while the phase shift stays at $50 \sim 60^\circ$ at most[15, 29, 30]. A similar distant complex pole would be found in the (1/2,0) channel, because the role of the ρ and K^* exchange and the behavior of the phase shift are quite similar to the ones in the (0,0) channel. Another example is the unitarized current algebra result[20, 31], which gives a pole at $\sqrt{-i16\pi}f_\pi = 463 - i463$ MeV. An inverse example is the linear σ model unitarized by the Padé [1,1] approximation applied to the perturbation series up to the one-loop level[32]. In this model the physical σ mass at which the phase shift crosses 90° is set near the ρ meson mass, but the complex poles in the unphysical sheet are found at near $(500 - 300\text{i})$ MeV. These values are close to the ones in the ρ exchange model and the unitarized current algebra, but the physics on the real axis is quite different from each other. The origin of the σ pole is quite different from the one of a pole near the real axis such as the ρ meson pole. It would be misleading, therefore, if we easily attribute any distant complex pole to the existence of an unstable meson state.

There is an argument to relate the $t-$channel ρ meson exchange with the $s-$channel σ resonance through the concept of the duality between the Regge pole exchange and the direct channel resonance[23, 27, 28]. This argument seems to be introduced so that the complex pole found in the ρ exchange amplitude could be regarded as a root of σ in the $s-$channel. If the $\pi^+\pi^- \to \pi^+\pi^-$ amplitude is expressed by the single Veneziano amplitude $V(s,t)$ in the Veneziano model[33], the amplitude in the physical region near the pole at $s \sim M_\rho^2 \sim M_\sigma^2$ is dominated not by the $t-$channel exchange term, $\sim g^2(s+t)/(M_\rho^2 - t)$ but the $s-$channel pole term, $\sim g^2(s+t)/(M_\rho^2 - s)$, and the both expressions cannot be added in order to avoid the double counting. Thus, it may be in trouble to add the ρ meson exchange amplitude to the σ pole term in the $s-$channel. Rather,the [1,1] Padé approximant applied to the linear sigma model without the ρ meson exchange[32] or the meson exchange model without the $s-$channel σ pole[14] would be consistent with the duality.

The duality would work severely for the models containing the explicit σ field or the σ pole besides the ρ field in the theory. But the exchanged object in the above models is not any Regge pole but merely a simple pole, and it is doubtful whether the complex pole found in the ρ exchange amplitude represents really the σ meson in the $s-$channel as discussed previously. If the model does not contain the σ field as an independent degree of freedom, and if the mass enhancement peaked at 500 MeV, which may be called σ state, comes from the two-pion correlation as the vacuum fluctuation owing to the spontaneous chiral symmetry breaking, it would need careful studies to understand the duality between the Regge pole exchange and the σ enhancement.

We have argued the two-meson scattering processes within one of the unitarized chiral perturbation theories in this note and obtained rather unpopular conclusions on the scalar meson spectroscopy. There are many interesting phenomena such as the production and decay processes including the low mass scalar "mesons" in order to reveal the nature of them. The confirmation of our conclusion and the consistency check with various processes should be pursued.

References

[1] G. Grayer et al., Nucl. Phys. **B75**(1974),189; B. Hyams et al., Nucl. Phys. **B64**(1973),134; M. J. Losty et al., Nucl. Phys. **B69**(1974),189; P. Estabrooks and A. D. Martin, Nucl. Phys. **B79**(1975), 301; V. Srinivasan et al., Phys. Rev. **D12**(1975), 681; L.Rosselet et al., Phys. Rev. **D15**(1977), 574; W. Hoogland et al., Nucl.Phys. **B126**(1977),109.

[2] R. Kamainski, L. Lesniak and K. Ribicki, C Phys. **C7**(1997), 79. R. Kaminski

[3] D. E. Groom et al., The Europian Phys. J. C15(2000), 1.

[4] D. Alde et al., GAMS Collaboration hep-ph/9712009 v2. C. Amsler et al., Phys. Lett. **B355**(1995), 425. D. Barberis et al., Phys. Lett.**B488**(2000), 225.

[5] R. Mercer et al., Nucl. Phys, **B32**(1971), 381; H.H. Bingham et al., Nucl. Phys, **B41**(1972),1; D. Linglin et al., Nucl. Phys, **B57**(1973),64; M. J. Matision et al., Phys. Rev. **D9**(1974), 1872; S. L. Baker et al., Nucl. Phys, **B99**(1975), 211; P. Estabrooks et al., Nucl. Phys, **B133**(1978), 490.

[6] A.Dobado and J.R. Pelàez, Phys. Rev. **D56**(1997), 3057.

[7] T. Hannah, Phys. Rev. **D54**(1996),4654; Phys. Rev. **D55**(1997), 5613.

[8] F.Guerrero and J.A. Oller, Nucl. Phys. **B537**(1999), 459; J. A. Oller, Erratum Nucl. Phys. **B602**(2001), 641.

[9] J.A. Oller, E. Oset, J.R. Pelàez, Phys. Rev. **D59**(1999), 074001; Errattum Phys. Rev. **D60**(1999), 09906; Phys. Rev. **D62** (2000),114017.

[10] A. Goméz Nicola and J.R. Pelàez, hep-ph/0109056.

[11] R.H.Dalitz and S.F. Tuan, Ann. Phys.**3**(1960), 307.

[12] Y. Fujii and M. Uehara, Prog. Theor. Phys. Suppl. **No. 21**(1962), 138.

[13] J. Weinstein and J. Isgur, Phys. Rev.**D41**(1990), 2236.

[14] D. Lhse, J.W. Durso, K. Hollinde and J. Speth, Nucl. Phys. **A516** (1990),513.

[15] G. Janssen, B.C. Pearce, K. Hollinde and J. Speth, Phys. Rev. **D52** (1995), 2690.

[16] J. Gasser and H. Leutwyler, Nucl. Phys. **B250** (1985), 465.

[17] V. Bernard, N. Kaiser and U-M. Meissner, Nucl. Phys. **B357** (1991), 129.

[18] G. Ecker, hep-ph/0011026.

[19] M. Boglione and M.R. Pennington, Z. Phys.**C75** (1997), 113.

[20] G Colangele, J. Gasser and H. Leutweyler, Nucl. Phys. **B603** (2001),125.

[21] J. Winstein and N. Isgur, Phys. Rev, **D43** (1991), 95.

[22] S.N. Cherry and M.R. Pennington, Nucl.Phys. **B** (2001), .

[23] Summary talk in *Proceedings of YITP Work Shop on Possible Existence of the $\sigma-$meson and its Implications to Hadron Physics*, Kyoto(2000).

[24] C. Rigenbach, J.F. Donogue, J. Gasser and B. Holtein, Phys. Rev. **D43** (1991),127.

[25] T-P. Cheng and L-F. Li,*Gauge theory of elementary particle physucs*, Oxford Univ. Press, New York(1984)

[26] J. Nieves and E. Ruiz Arriola, Nucl. Phys. bf A679 (2000), 57.

[27] M.R Pennington, hep-ph/9905241.

[28] P. Minkowski and W. Ochs, hep-ph/9905250.

[29] B.S. Zou and D.V. Bugg, Phys. rev. **D50** (1994), 591.

[30] Long Li, Bin Song Zou and Guang-lie Li, Phys. Rev. **D63**(2001), 074003.

[31] D. Jido, T. Hatsuda and T. Kunihiro, Phys. Rev. **D63** (2001), 011901.

[32] J.L. Basdevant and B.W. Lee, Phys. rev. **D2** (1970),1680.

[33] G. Veneziano, Nuovo Cimento **57**A(1968), 190.